

Journal of Materials Chemistry A

Accepted Manuscript



This is an *Accepted Manuscript*, which has been through the Royal Society of Chemistry peer review process and has been accepted for publication.

Accepted Manuscripts are published online shortly after acceptance, before technical editing, formatting and proof reading. Using this free service, authors can make their results available to the community, in citable form, before we publish the edited article. We will replace this *Accepted Manuscript* with the edited and formatted *Advance Article* as soon as it is available.

You can find more information about *Accepted Manuscripts* in the [Information for Authors](#).

Please note that technical editing may introduce minor changes to the text and/or graphics, which may alter content. The journal's standard [Terms & Conditions](#) and the [Ethical guidelines](#) still apply. In no event shall the Royal Society of Chemistry be held responsible for any errors or omissions in this *Accepted Manuscript* or any consequences arising from the use of any information it contains.

Cite this: DOI: 10.1039/c0xx00000x

www.rsc.org/MaterialsA

Facile preparation of ZnGa₂O₄ photonic crystals with enhanced light absorption and photocatalytic activity

Xiaofang Li, Xiaoyun Zhang, Xiuzhen Zheng, Miao He, Peng Wang, Yu Shao and Danzhen Li*

Received (in XXX, XXX) Xth XXXXXXXXXX 20XX, Accepted Xth XXXXXXXXXX 20XX

DOI: 10.1039/b000000x

Photonic crystals of multiple metal oxides with highly ordered structure and unique photonic effects have presented a prospective application in the design of photocatalysts. In this study, a facile method was developed to prepare pure ZnGa₂O₄ photonic crystals with highly ordered skeleton structure at a relatively lower temperature (500 °C). Due to the facilitated mass transport in the highly-ordered channel, the as-prepared ZnGa₂O₄ photonic crystals exhibited better photocatalytic activities towards methyl orange degradation compared to those of porous ZnGa₂O₄ and ZnGa₂O₄ nanocrystals. By changing the pore diameters in the structure, slow photon effect on the blue edge of photonic band gap could be observed, which consequently enhanced the electronic band absorption over ZnGa₂O₄ photonic crystals with a pore diameter of 180 nm and further improved the corresponding photocatalytic activity. Furthermore, the degradation mechanism over ZnGa₂O₄ photonic crystals was discussed. The preparation of ZnGa₂O₄ photonic crystals in this study provided an experimental guidance for developing ternary metal oxide photonic crystals with enhanced light absorption and photocatalytic activities.

1. Introduction

As an efficient and economical technique, heterogeneous photocatalysis has attracted much attention in the remediation of organics contaminated environment.¹⁻⁷ The interaction between incident photons and photocatalysts was the primary process in the photocatalytic reactions. Thus, great effort has been devoted to design photocatalysts which could exhibit enhanced light absorption around their electronic band gaps.⁸⁻¹² Recently, photonic crystals (PCs) have attracted great interest in the design of photocatalysts due to the advantage of their ordered structures and photonic effects.¹³⁻¹⁵ The three-dimensional ordered macroporous structure in the PCs could facilitate the transfer of reactant molecules in the interconnected pore channels. The photonic effects at the edge of photonic band gap, termed as slow photon effect,¹⁶ slowed the propagation velocity of photons in the photocatalysts, and then intensified the light absorption of the photocatalysts. Based on the unique properties, PCs photocatalysts were expected to achieve remarkably enhancement in their various photocatalytic performances.

Up to date, the most reported TiO₂ PCs exhibited significantly increased photocatalytic activities compared with conventional TiO₂ nanocrystals,¹⁷⁻²⁴ but they still had low photocatalytic efficiencies. In our previous study, β-Ga₂O₃ PCs were reported to have comparable photocatalytic activities to that of commercial TiO₂ (P25, Degussa Co.) towards various organic pollutions,²⁵ which indicated the potentially high photocatalytic efficiencies over Ga-based oxides PCs. Furthermore, it was found that the photocatalytic activity of Ga₂O₃ could be enhanced by

introducing foreign ions such as Zn²⁺.^{26, 27} Therefore, to explore Ga-based oxides PCs with enhanced photocatalytic efficiencies, the ternary metal oxide ZnGa₂O₄ PCs were designed in this study. Compared with single-metal oxides PCs, two difficulties existed in the preparation of ternary metal oxides PCs. The first one was the appropriate choice of the complex precursor to produce ternary metal oxides with desired metal ratio.²⁸⁻³⁰ The cations in the complex precursor should be homogeneously dispersed to obtain porous ternary metal oxides with pure phases. The second problem was the thermal stability of the PCs structure.³¹ High calcination temperatures were usually necessary for the crystallization of ternary metal oxides. However, the porous structure of the PCs might collapse upon high-temperature treatment. Therefore, the preparation of ternary metal oxides PCs was still challenging.

Herein, we described a facile route to synthesize the ZnGa₂O₄ PCs for the first time. The pure ZnGa₂O₄ PCs could be obtained at a relatively lower temperature (500 °C) by using acetylacetonate-complexed metal ion precursors. And the photonic band gap of the as-prepared samples could be modulated by changing their pore diameters. The photocatalytic activities of the ZnGa₂O₄ PCs for the degradation of methyl orange were investigated in detail under UV light irradiation, including the photonic effect arising from the highly-ordered structure in the ZnGa₂O₄ PCs and the catalytic stability of the ZnGa₂O₄ PCs. Furthermore, the photocatalytic mechanism for the degradation of methyl orange over the ZnGa₂O₄ PCs was also discussed. Our results might allow us to provide an experimental guidance for developing

ternary metal oxide PCs with enhanced light absorption and photocatalytic activities.

2. Experimental section

2.1. Materials

Styrene (99%) was obtained from Aldrich Co., and was further washed by 5 wt% NaOH (A.R., Sinopharm Chemical Reagent Co. (SCRC)) aqueous solution to remove the stabilizing agent (*p*-tert-butylcatechol). Potassium peroxydisulfate (A.R., SCRC) was recrystallized before use. Gallium nitrate ($\text{Ga}(\text{NO}_3)_3 \cdot x\text{H}_2\text{O}$) was purchased from Shanghai Longjin Industry & Trade Co.. Zinc nitrate hexahydrate and ($\text{Zn}(\text{NO}_3)_2 \cdot 6\text{H}_2\text{O}$, A.R., SCRC) and acetylacetone (A.R., SCRC) were used directly as the precursor.

2.2. Preparation of polystyrene sphere templates

The colloidal polystyrene (PS) spheres with various sphere diameters were synthesized using a typical emulsion polymerization according to the literature (Detailed experiments see in Supporting information).³² Then, the PS sphere template was deposited on the glass substrate by a solvent evaporation method. In this method, the substrate was immersed vertically into a colloidal PS spheres suspension with a concentration of 0.05 wt% in a 50 mL beaker. Then the beaker was kept at 50 °C for about 2 days in an oven until the water was fully evaporated, leaving a PS sphere template on the substrate. Before use, the glass substrate (1.9×1.3 cm) was rinsed by soaking in a mixture of $\text{H}_2\text{SO}_4/\text{H}_2\text{O}_2$ solution with the volume ratio of 7:3 for 24 h, and then washed with deionized water and dried in a nitrogen stream with a flow rate of 100 mL/min.

2.3. Preparation of ZnGa_2O_4 PCs

The ZnGa_2O_4 PCs with different pore diameters were synthesized following a dip-coating infiltration method by using the as-prepared PS templates.³³ Firstly, the amorphous complex precursor was produced according to the literature.³⁴ Typically, 4 mmol of $\text{Ga}(\text{NO}_3)_3 \cdot x\text{H}_2\text{O}$ was dissolved in 8 mL of ethanol, and then 2 mL of acetylacetone were added. Then 2 mmol of $\text{Zn}(\text{NO}_3)_2 \cdot 6\text{H}_2\text{O}$ was dissolved in the above solution. The resulting mixture was kept at 50 °C for 12 h until it turned into a light yellow transparent solution. Secondly, the as-prepared PS templates were immersed vertically into the liquid precursor for 1 min to fill the void volume of the templates completely. At last, the infiltrated PS templates were dried in air at room temperature and calcined at given temperatures in air for 5 h with a heating rate of 1 °C/min to remove the PS templates and obtain the ZnGa_2O_4 PCs.

2.4. Characterization

The morphologies of the obtained samples were observed by a field-emission scanning electron microscopy (FESEM, Hitachi SU8000, operated at an accelerating voltage of 5 kV). X-ray diffraction (XRD) patterns of the samples were measured by a Bruker D8 Advance X-ray diffractometer at 40 kV and 40 mA with Cu K α radiation. TG spectra were obtained by a STA449F3 thermogravimetric analyzer (NETZSCH Co.). Reflection spectra of the samples were collected by Cary 500 UV-vis-NIR spectrophotometers with BaSO_4 as a reflectance standard. The generation of $\cdot\text{OH}$ radical was investigated by the

photoluminescence (PL) technique with terephthalic acid (TA) as a probe molecule. In this method, TA could react with the $\cdot\text{OH}$ radical to form a high fluorescent product, 2-hydroxyterephthalic acid, which could be detected by fluorescence spectrum (excitation wavelength: 312 nm, emission wavelength: 426 nm).³⁵ The PL spectra were obtained on an Edinburgh FL/FS900 spectrophotometer. The *N,N*-diethyl-*p*-phenylenediamine (DPD) method was employed for the detection of H_2O_2 . This method was based on the horseradish peroxidase (POD)-catalyzed oxidation of DPD by H_2O_2 . The sequence of reaction led to form a pink colored $\cdot\text{DPD}^+$ radical cation. This radical cation had the absorption at 510 and 551 nm, respectively.^{37,38}

2.5. Test of photocatalytic activity

The photocatalytic degradation of methyl orange (MO) in liquid phase were carried out in a 10 mL of quartz cell. Two 4 W UV lamps with a wavelength centered at 254 nm (Philips Co., TUV 4W/G4 T5) were used as the irradiation source. The spectrum was shown in Fig. S1 and the UV band output was shown in Table S1. Typically, the ZnGa_2O_4 PCs were immersed vertically in 10 mL of the MO aqueous solution (1.5×10^{-5} mol/L). Prior to irradiation, the solution was stirred for 20 min to reach adsorption-desorption equilibrium between the sample and MO. As the reaction proceeded, 3 mL of MO aqueous solution were taken at a certain time interval. The concentration of MO was analyzed by monitoring the absorbance at $\lambda_{\text{max}} = 464$ nm in UV-vis spectrum with a Cary 50 UV-vis spectrophotometer (Varian Co.). Moreover, the total organic carbon (TOC) values of the MO aqueous solution were detected by a Shimadzu TOC-V_{CPH} total organic carbon analyzer.

3. Results and discussion

3.1. SEM and XRD analysis

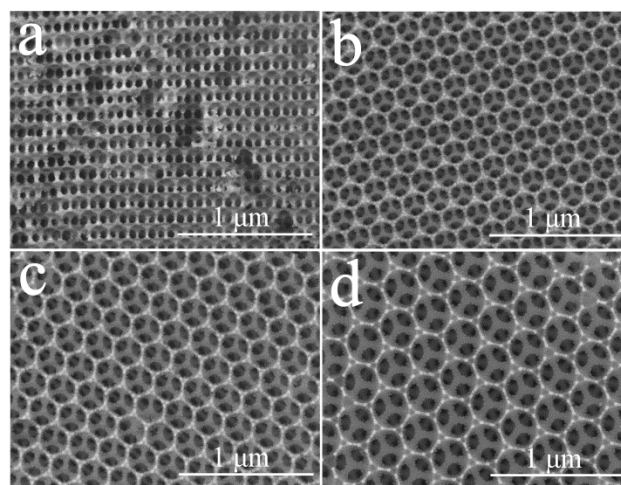


Fig. 1 SEM images of the ZnGa_2O_4 PCs with different pore diameters prepared at 500°C: (a) ZG PCs/145, (b) ZG PCs/180, (c) ZG PCs/225, and (d) ZG PCs/280.

SEM images of the as-prepared PS templates were shown in Fig. S2. The PS sphere templates with various PS sphere diameters of 190, 240, 300 and 380 nm could be obtained by using 1.8, 2.4, 4.2 and 7.2 mL of styrene as the monomer, respectively. The ZnGa_2O_4 PCs with different pore diameters were synthesized by

using the as-prepared PS templates. Fig. 1 showed SEM images of the ZnGa_2O_4 PCs prepared at 500 °C. It could be observed that the ZnGa_2O_4 PCs well duplicated the highly ordered structure of PS template to form an ordered skeleton structure. The average pore diameters of the ZnGa_2O_4 PCs were 145, 180, 225 and 280 nm, respectively. And the film thicknesses of the ZnGa_2O_4 PCs were roughly evaluated to be $\sim 1 \mu\text{m}$ by the cross-sectional SEM in Fig. S3. For the sake of simplicity, the as-prepared PCs with different pore diameters were denoted as ZG PCs/145, ZG PCs/180, ZG PCs/225 and ZG PCs/280, respectively. Moreover, SEM images of the sample ZG PCs/180 prepared at 400 °C and 600 °C were shown in Fig. S4. As it could be seen, the integrated structure collapsed at 600 °C due to the high temperature calcination. XRD patterns of the ZnGa_2O_4 PCs with different pore diameters prepared at 500 °C were shown in Fig. 2. All diffraction peaks in the patterns could be identified as a single cubic phase of ZnGa_2O_4 with spinel structure (JCPDS card no. 086-0415). The peaks at 2θ about 18.42, 30.30, 35.70, 37.34, 43.39, 53.84, 57.39 and 63.03° could be indexed to the diffraction peaks of the (111), (220), (311), (222), (400), (422), (511) and (440) crystal planes of ZnGa_2O_4 , respectively. Furthermore, XRD patterns of the sample ZG PCs/180 prepared at 400 °C and 600 °C were also shown in Fig. 3. It could be observed that the calcination temperature more than 400 °C was necessary to obtain ZnGa_2O_4 . The intensities of the diffraction peaks in the XRD patterns were significantly enhanced as the calcination temperature increased to 500 °C, indicating an improved crystallinity of ZnGa_2O_4 . Exceeding 500 °C, no obvious enhancement in peak intensities could be observed. Moreover, the TG analysis results indicated that the decomposition of the PS template and the formation of ZnGa_2O_4 could be achieved at 500 °C (see Fig. S5). This further confirmed that pure ZnGa_2O_4 PCs could be obtained at an optimal temperature of 500 °C in this work.

For comparison, a porous ZnGa_2O_4 film was prepared at 500 °C as a reference by using the disordered PS template. Furthermore, a ZnGa_2O_4 nanocrystal film was also prepared by employing the same method but without the PS template on the substrate. The as-prepared samples were denoted as ZG/mix and ZG NCs, respectively. SEM images of samples ZG/mix and ZG NCs were displayed in Fig. S6. A disordered structure was observed for sample ZG/mix, the sample ZG NCs showed the

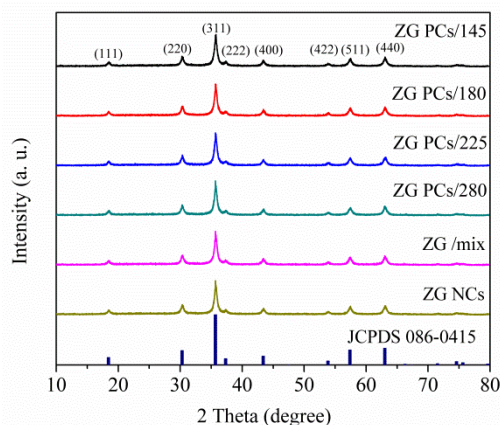


Fig. 2 XRD patterns of the ZnGa_2O_4 PCs with different pore diameters prepared at 500 °C.

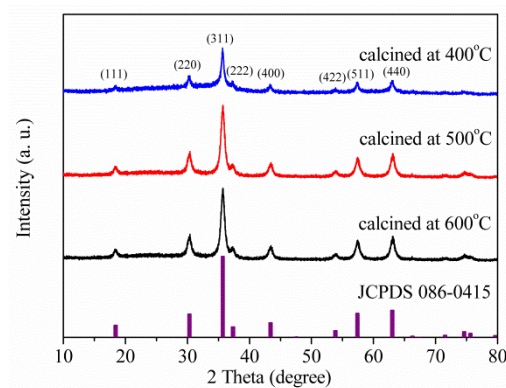


Fig. 3 XRD patterns of the sample ZG PCs/180 prepared at different temperatures.

nature of nanocrystals. Furthermore, the results of the XRD patterns confirmed that samples ZG/mix and ZG NCs were pure ZnGa_2O_4 . (see Fig. 2)

3.2. Reflection spectra and absorption spectra

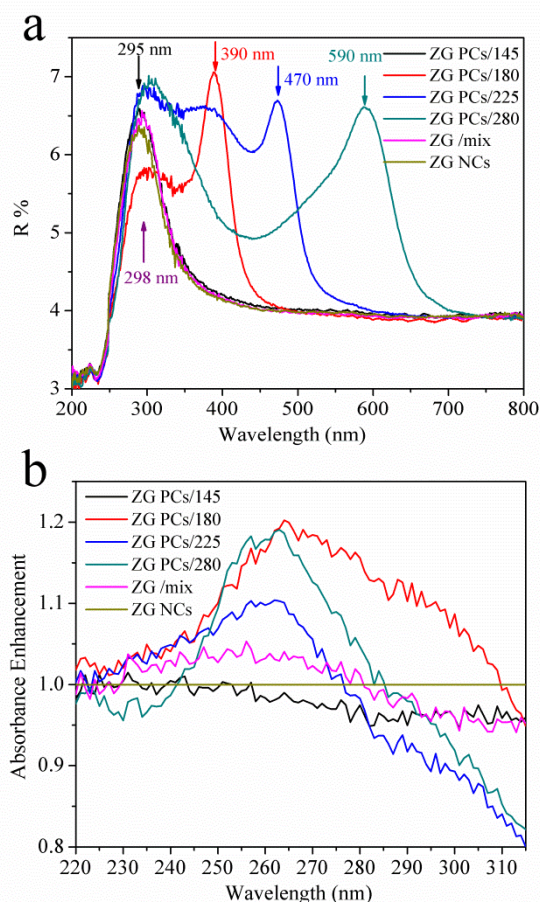


Fig. 4 (a) Reflection spectra of the ZnGa_2O_4 PCs with different pore diameters prepared at 500 °C. (b) Absorption enhancement spectra as a function of the wavelength for the as-prepared samples.

Fig. 4a showed the reflection spectra of the ZnGa_2O_4 PCs with different pore diameters prepared at 500 °C. All samples exhibited a reflection peak at about 298 nm, corresponding to a band gap of 4.2 eV. This could be attributed to the electronic band gap of ZnGa_2O_4 . Furthermore, the reflection peaks of the

photonic band gaps for the ZnGa_2O_4 PCs were also observed in the reflection spectra. It was noted that the photonic band gaps of the as-prepared samples could be modulated by changing the pore diameters of the ZnGa_2O_4 PCs. As shown in Fig. 4a, the photonic band gaps located at 295, 390, 470 and 590 nm can be observed for samples ZG PCs/145, ZG PCs/180, ZG PCs/225 and ZG PCs/280, respectively. For sample ZG PCs/145, the photonic band gap was located at 295 nm. This indicated that the photonic band gap of sample ZG PCs/145 would reflect the light with a wavelength of 295 nm, and therefore could suppress the light absorption of sample ZG PCs/145.¹⁴ However, it was found that the electronic band gap of ZnGa_2O_4 overlapped the blue edge of the photonic band gap for sample ZG PCs/180. As a result, the light absorption of sample ZG PCs/180 could be enhanced due to the slow photon effect.³⁹⁻⁴² While the photonic band gaps of the as-prepared samples were away from the electronic band gap of ZnGa_2O_4 , the slow photon effect would be weakened. These might affect the photocatalytic activities of the as-prepared samples, which would be discussed below.

In order to verify that slow photon effect had an enhancement effect on the light absorption, the reflectance spectra of the ZnGa_2O_4 PCs were transformed into the absorption spectra by using the Kubelka-Munk function and the resultant absorption spectra were shown in Fig. S7, as well as ZG/mix and ZG NCs. Furthermore, the absorption spectra of the ZnGa_2O_4 PCs and sample ZG/mix were normalized to that of sample ZG NCs and the resultant absorption enhancement spectra were shown in Fig. 4b. It was obviously that there was an absorption enhancement located at 265 - 310 nm in the electronic band gap absorption region for sample ZG PCs/180. The enhancement could be attributed to the slow photon effect, which slowed the light propagation in the ZnGa_2O_4 PCs and thus reinforced the interaction between photons and ZnGa_2O_4 . By contrast, a suppressed absorption could be observed over the sample ZG PCs/145 due to the photonic band gap reflection, which reflected partial light in the electronic band gap region and declined the electronic band gap absorption.

3.3. Photocatalytic degradation of MO

To evaluate the slow photon effect on the photocatalytic activity of PCs, the photocatalytic activities of the ZnGa_2O_4 PCs prepared at 500 °C for the degradation of MO under UV light irradiation ($\lambda = 254$ nm) were shown in Fig. 5. For comparison, the degradation of MO over the samples ZG/mix and ZG NCs were also carried out under the same conditions. As shown in Fig. 5, the ZnGa_2O_4 PCs and sample ZG/mix, which were porous samples, exhibited higher catalytic activities than that of sample ZG NCs. Their higher catalytic activities could be ascribed to the enhanced light harvest resulted from the light scattering in the porous structures and the facilitated mass transport in the interconnected channels. Further, as compared to the sample ZG/mix, the ZnGa_2O_4 PCs showed better photocatalytic activities for the degradation of MO. The enhanced photocatalytic activities could be attributed to that the highly ordered channels with excellent connectivity efficiently facilitated the mass transport on the reaction sites.

It was noted that the sample ZG PCs/180 exhibited the highest photocatalytic activity in the ZnGa_2O_4 PCs, and its catalytic activity was also higher than that of commercial TiO_2 (P25, Degussa Co.) under the same condition. Up to 96% of MO was

degraded and the TOC removal rate was 47.5% for the sample ZG PCs/180 after 75 min of UV light irradiation. As shown in Fig. 4, the enhanced electronic band gap absorption was observed over sample ZG PCs/180 due to the slow photon effect. This led to more photoinduced carriers generated in the ZnGa_2O_4 , and consequently sample ZG PCs/180 exhibited high photocatalytic activity. When the photonic band gaps of the ZnGa_2O_4 PCs were away from the electronic band gap of ZnGa_2O_4 , the slow photon effect on enhancing the electronic band gap absorption for the as-prepared samples would be weakened. As a result, samples ZG PCs/225 and ZG PCs/280 showed relatively lower activities as compared to the sample ZG PCs/180. Under this condition, the photocatalytic activity was also related with the pore diameter of ZnGa_2O_4 PCs, which has been proven by our previous work.^{24,33} Therefore, sample ZG PCs/280 showed better photocatalytic activity than that of ZG PCs/225. Furthermore, it was found that the electronic band gap absorption of the sample ZG PCs/145 was suppressed by the photonic band gap reflection (see Fig. 4). Therefore, the photocatalytic activity of sample ZG PCs/145 was lower than those of other ZnGa_2O_4 PCs.

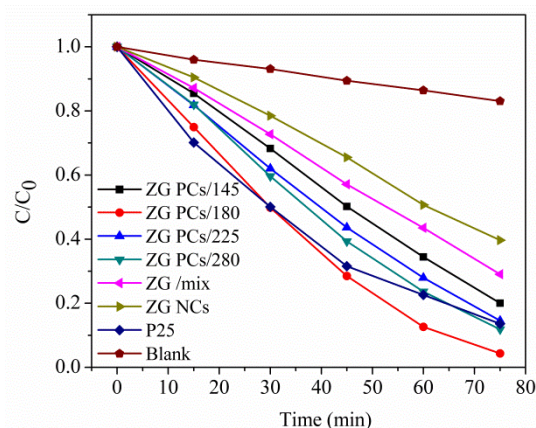


Fig. 5 Photocatalytic activities of the ZnGa_2O_4 PCs prepared at 500 °C for the degradation of MO under UV light irradiation ($\lambda = 254$ nm).

Moreover, the effect of calcination temperature on the photocatalytic activities of the ZnGa_2O_4 PCs for the degradation of MO was investigated. As shown in Fig. 6, negligible catalytic activity could be observed for the sample ZG PCs/180 prepared at 400 °C, which was probably due to its low crystallinity as shown in XRD patterns (see Fig. 3). Furthermore, the sample ZG PCs/180 prepared at 600 °C showed lower photocatalytic activity than that prepared at 500 °C. The decrease in the catalytic activity was attributed to the collapse of the ordered photonic crystal structure (see Fig. S4), thus weakening the advantages of slow photons, multiple scattering, and continuous pore channels. This result further verified that the optimal calcination temperature was 500 °C for the ZnGa_2O_4 PCs.

It was widely regarded that the stability of a catalyst was a very important factor for its practical applications. As shown in Fig. 7, the photocatalytic activity of a typical sample (ZG PCs/180) did not obviously decrease in the recycling experiment. Its catalytic activity can keep at ~ 100% in the 5th cycle of testing. The result suggested that the ZnGa_2O_4 PCs had excellent photocatalytic stability for the MO degradation under UV light irradiation.

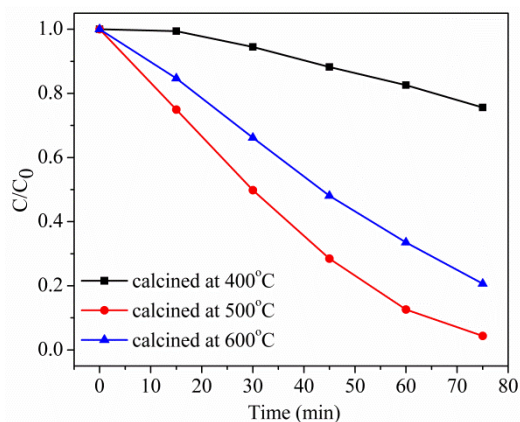


Fig. 6 Photocatalytic activities of the sample ZG PCs/180 prepared at different temperatures for the degradation of MO.

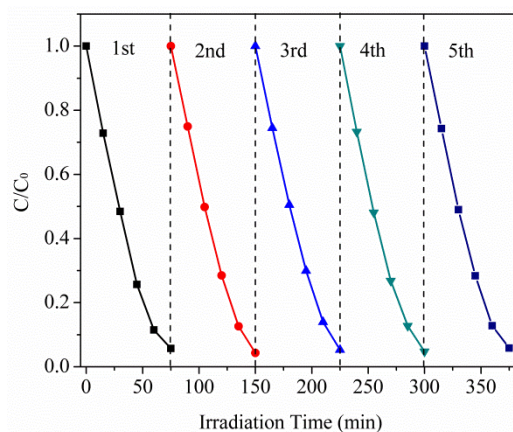


Fig. 7 Reusability of sample ZG PCs/180 for the photocatalytic degradation of MO.

3.4. Mechanism

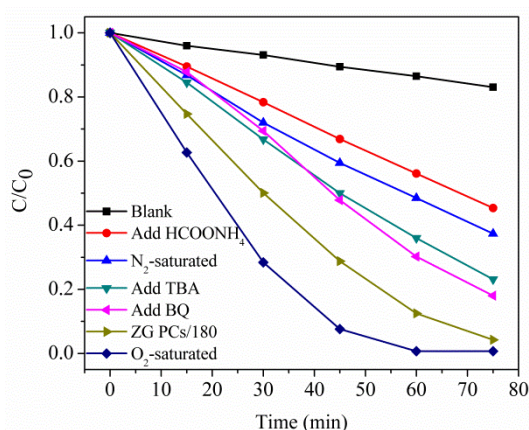


Fig. 8 Photocatalytic degradation of MO over sample ZG PCs/180 under different conditions.

As a part of this work, the reaction mechanism of the photocatalytic degradation of MO over the ZnGa_2O_4 PCs was investigated in detail. Generally, photoinduced holes, $\cdot\text{OH}$ radicals and $\cdot\text{O}_2^-$ radicals were considered to be main active species for the organic pollutants degradation. To explore a better approach to understand the degradation of MO over the ZnGa_2O_4 PCs, different types of scavengers were used in this work. As shown in Fig. 8, the addition of HCOONH_4 as a hole-scavenger

significantly inhibited the photocatalytic activity, which indicated that the photoinduced holes played the most important role in the degradation of MO. Furthermore, *tert*-butyl alcohol (TBA) as a scavenger for $\cdot\text{OH}^{\text{H}}$ and benzoquinone (BQ) as scavenger for $\cdot\text{O}_2^{\text{H}}$ suppressed the photocatalytic activity to a lesser extent. It was found that the photocatalytic activity of sample ZG PCs/180 could be improved observably when the reaction was carried out under O_2 atmosphere (see Fig. 8). The presence of O_2 could trap the photoinduced electrons ($e^- + \text{O}_2 \rightarrow \cdot\text{O}_2^-$). As a result, more photoinduced holes, $\cdot\text{OH}$ radicals and $\cdot\text{O}_2^-$ radicals could be generated, and then participate in the degradation of MO. By contrast, sample ZG PCs/180 showed low catalytic activity for the degradation of MO under N_2 atmosphere. This could be attributed to that the N_2 atmosphere aggravated the recombination of photoinduced carriers. These results further indicated that the

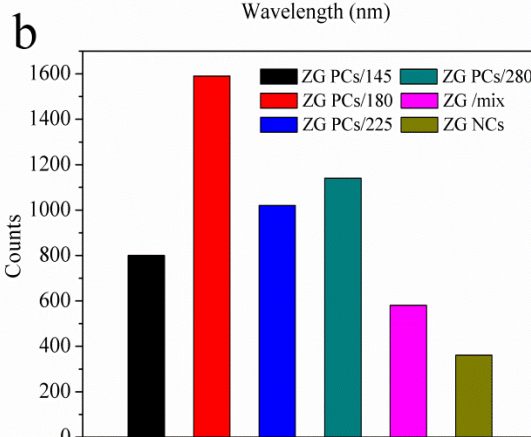
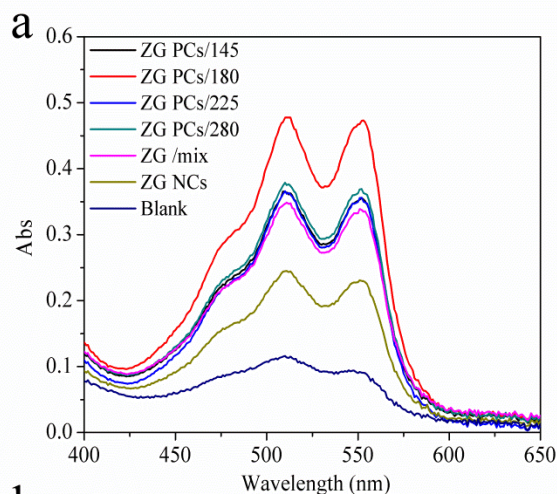


Fig. 9 (a) UV-vis spectra of the DPD/POD reagent reacted with the produced H_2O_2 and (b) the $\cdot\text{OH}$ -trapping PL intensity of the TA aqueous solution at 426 nm in the presence of different ZnGa_2O_4 samples after 75 min of UV light irradiation.

photoinduced holes, $\cdot\text{OH}$ radicals and $\cdot\text{O}_2^-$ radicals were the important species in the degradation of MO over the ZnGa_2O_4 PCs.

Furthermore, the formation process of the $\cdot\text{OH}$ radicals was investigated in detail. Generally, the photoinduced holes (h^+) of the ZnGa_2O_4 PCs could react with water to produce the $\cdot\text{OH}$ radicals ($h^+ + \text{H}_2\text{O} \rightarrow \cdot\text{OH} + \text{H}^+$; $E_{\text{valence band}}(\text{ZnGa}_2\text{O}_4) = 2.95 \text{ V vs. SHE at pH 7}$; $E(\cdot\text{OH}/\text{H}_2\text{O}) = 2.27 \text{ V vs. SHE at pH 7}$). In

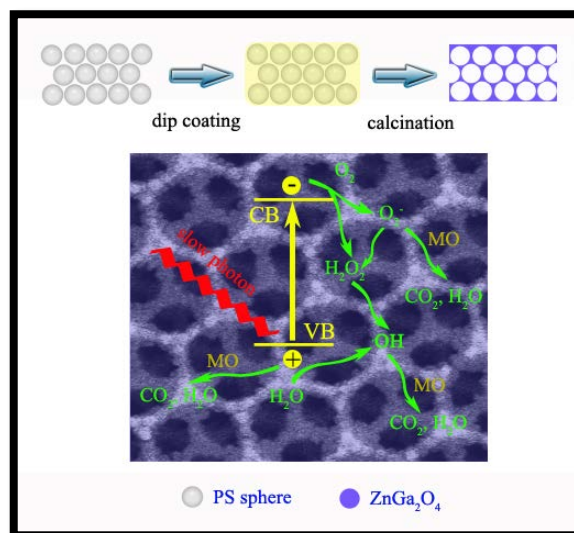
this work, as shown in Fig. 9a, the presence of H₂O₂ was also detected in the photocatalytic reaction by the DPD method. The formation of H₂O₂ could be as a consequence of the reduction reactions by the photoinduced electrons (e⁻) of ZnGa₂O₄ (e⁻ + O₂ → ·O₂⁻; 2 e⁻ + O₂ + 2H⁺ → H₂O₂; ·O₂⁻ + ·O₂⁻ + 2H⁺ → H₂O₂ + O₂⁴⁷). H₂O₂ would further decompose into the ·OH radicals (H₂O₂ + hν → 2 ·OH). Therefore, these results revealed that there were two ways in the formation the ·OH radicals for the ZnGa₂O₄ PCs: the first one was the reaction between the photoinduced holes and water molecules; the second one was the decomposition of H₂O₂.

It was noted that the amount of H₂O₂ in the sample ZG PCs/180 system was higher than other sample systems (Fig. 9a). Moreover, the presence of ·OH radicals was proved by the PL-TA method in this work. The peak at 426 nm in Fig. S8 indicated the formation of ·OH. As shown in Fig. 9b, the ·OH-trapping PL intensity at 426 nm over sample ZG PCs/180 was relatively stronger as compared to other ZnGa₂O₄ PCs. The more H₂O₂ and ·OH radicals produced in the aqueous solution under UV-light irradiation could be attributed to the slow photon effect for sample ZG PCs/180. These results might further explain why sample ZG PCs/180 showed the highest photocatalytic activity for the degradation of MO.

On the basis of the above experimental results, the synthesis process of the ZnGa₂O₄ PCs and the proposed mechanism for the photocatalytic degradation of MO over the ZnGa₂O₄ PCs were illustrated in Scheme 1. When the ZnGa₂O₄ PCs were irradiated under UV light, the slow photon effect on the edge of photonic band gap enhanced the electronic band absorption. As a result, more photoinduced carriers were created, and then migrated to the surface of the photocatalyst to participate in the redox reactions. The photoinduced electrons on the conduction band (CB) were trapped by adsorbed molecular oxygen on the photocatalyst surface to produce ·O₂⁻ radicals and H₂O₂ molecules. The ·O₂⁻ radicals and H₂O₂ molecules would be converted into ·OH radicals by chain reactions. Furthermore, a part of photoinduced holes on the valence band (VB) could oxidize H₂O molecules to produce ·OH radicals. Photoinduced holes, ·OH radicals and ·O₂⁻ radicals had strong oxidative abilities, and therefore they could degrade MO into CO₂ and H₂O.

4. Conclusion

In summary, we have developed a facile method to prepare the ZnGa₂O₄ PCs for the first time. The pure ZnGa₂O₄ PCs with highly ordered skeleton structure could be obtained at a relatively lower temperature (500 °C) by using acetylacetonate-complexed metal ion precursors. The as-prepared ZnGa₂O₄ PCs exhibited better photocatalytic activity towards the MO degradation compared to the porous ZnGa₂O₄ and ZnGa₂O₄ nanocrystals due to the facilitated mass transport in the highly-ordered channel. By changing the pore diameter of the ZnGa₂O₄ PCs, the slow photon effect could be observed over sample ZG PCs/180, which enhanced the electronic band absorption and further improved the corresponding photocatalytic activity. Excellent photocatalytic stability could also be achieved over the ZnGa₂O₄ PCs. Further experimental results indicated that photoinduced holes, ·OH radicals and ·O₂⁻ radicals were the main active species responsible for the degradation of MO for the ZnGa₂O₄ PCs.



Scheme 1 The synthesis process of the ZnGa₂O₄ PCs and the proposed mechanism for the photocatalytic degradation of MO over the ZnGa₂O₄ PCs.

Acknowledgements

This work was financially supported by the National Natural Science Foundation of China (21173047, 21373049 and 21033003), and 973 Program of China (2013CB632405).

Notes and references

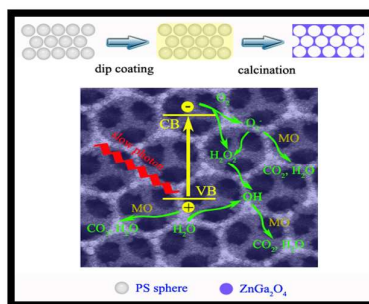
Research Institute of Photocatalysis, State Key Laboratory of Photocatalysis on Energy and Environment, Fuzhou University, Fuzhou 350002, P. R. China. Tel & Fax: (+86)591-83779256; E-mail: dzli@fzu.edu.cn

† Electronic Supplementary Information (ESI) available: SEM images of the as-prepared PS sphere templates with different sphere diameters; Cross-sectional SEM images of the ZnGa₂O₄ PCs with different pore diameters prepared at 500 °C; SEM images of sample ZG PCs/180 prepared at different temperatures; TG analysis of the amorphous complex precursor, the PS sphere template and the precursor infiltrated PS spheres template; The SEM images of disordered PS sphere template, sample ZG NCs and sample ZG/mix; Absorption spectra of the as-prepared ZnGa₂O₄ PCs; The spectrum of the UV light (center wavelength λ = 254 nm); The UV band output of UV light (center wavelength λ = 254 nm); The ·OH-trapping PL spectra of the TA aqueous solution in the presence of sample ZG PCs/180. See DOI: 10.1039/b000000x/

1. D. Chatterjee and S. Dasgupta, *Journal of Photochemistry and Photobiology C: Photochemistry Reviews*, 2005, **6**, 186-205.
2. U. I. Gaya and A. H. Abdullah, *Journal of Photochemistry and Photobiology C: Photochemistry Reviews*, 2008, **9**, 1-12.
3. J. Herrmann, *Catalysis Today*, 1999, **53**, 115-129.
4. M. Wang, J. Iocozzia, L. Sun, C. Lin and Z. Lin, *Energy & Environmental Science*, 2014, **7**, 2182-2202.
5. M. Wang, L. Sun, Z. Lin, J. Cai, K. Xie and C. Lin, *Energy & Environmental Science*, 2013, **6**, 1211-1220.
6. M. Wang, L. Sun, J. Cai, P. Huang, Y. Su and C. Lin, *Journal of Materials Chemistry A*, 2013, **1**, 12082-12087.
7. Y. Hou, X. Li, X. Zou, X. Quan and G. Chen, *Environmental Science & Technology*, 2008, **43**, 858-863.

8. H. Irie, Y. Watanabe and K. Hashimoto, *The Journal of Physical Chemistry B*, 2003, **107**, 5483-5486.
9. Y. Hu, Y. Cao, P. Wang, D. Li, W. Chen, Y. He, X. Fu, Y. Shao and Y. Zheng, *Applied Catalysis B: Environmental*, 2012, **125**, 294-303.
10. Y. Lin, D. Li, J. Hu, G. Xiao, J. Wang, W. Li and X. Fu, *The Journal of Physical Chemistry C*, 2012, **116**, 5764-5772.
11. J. Wang, P. Wang, Y. Cao, J. Chen, W. Li, Y. Shao, Y. Zheng and D. Li, *Applied Catalysis B: Environmental*, 2013, **136-137**, 94-102.
12. L. Yu, Y. Huang, G. Xiao and D. Li, *Journal of Materials Chemistry A*, 2013, **1**, 9637.
13. J. I. Chen, G. Freymann, V. Kitaev and G. A. Ozin, *J Am Chem Soc*, 2007, **129**, 1196-1202.
14. J. I. L. Chen, G. von Freymann, S. Y. Choi, V. Kitaev and G. A. Ozin, *Advanced Materials*, 2006, **18**, 1915-1919.
15. J. I. L. Chen, G. von Freymann, S. Y. Choi, V. Kitaev and G. A. Ozin, *Journal of Materials Chemistry*, 2008, **18**, 369.
16. S. Nishimura, N. Abrams, B. A. Lewis, L. I. Halaoui, T. E. Mallouk, K. D. Benkstein, J. van de Lagemaat and A. J. Frank, *Journal of the American Chemical Society*, 2003, **125**, 6306-6310.
17. J. I. L. Chen and G. A. Ozin, *Journal of Materials Chemistry*, 2009, **19**, 2675.
18. L. I. Halaoui, N. M. Abrams and T. E. Mallouk, *The Journal of Physical Chemistry B*, 2005, **109**, 6334-6342.
19. G. Liao, S. Chen, X. Quan, H. Chen and Y. Zhang, *Environmental Science & Technology*, 2010, **44**, 3481-3485.
20. J. Liu, G. Liu, M. Li, W. Shen, Z. Liu, J. Wang, J. Zhao, L. Jiang and Y. Song, *Energy & Environmental Science*, 2010, **3**, 1503.
21. Y. Lu, H. Yu, S. Chen, X. Quan and H. Zhao, *Environmental Science & Technology*, 2012, **46**, 1724-1730.
22. G. I. Waterhouse, A. K. Wahab, M. Al-Oufi, V. Jovic, D. H. Anjum, D. Sun-Waterhouse, J. Llorca and H. Idriss, *Scientific reports*, 2013, **3**, 2849.
23. X. Zhang, Y. Liu, S.-T. Lee, S. Yang and Z. Kang, *Energy & Environmental Science*, 2014, **7**, 1409.
24. X. Zheng, S. Meng, J. Chen, J. Wang, J. Xian, Y. Shao, X. Fu and D. Li, *The Journal of Physical Chemistry C*, 2013, **117**, 21263-21273.
25. X. Li, X. Zhen, S. Meng, J. Xian, Y. Shao, X. Fu and D. Li, *Environmental Science & Technology*, 2013, **47**, 9911-9917.
26. Y. Sakata, Y. Matsuda, T. Nakagawa, R. Yasunaga, H. Imamura and K. Teramura, *ChemSusChem*, 2011, **4**, 181-184.
27. Y. Sakata, Y. Matsuda, T. Yanagida, K. Hirata, H. Imamura and K. Teramura, *Catal Lett*, 2008, **125**, 22-26.
28. M. Sadakane, T. Asanuma, J. Kubo and W. Ueda, *Chemistry of Materials*, 2005, **17**, 3546-3551.
29. M. Sadakane, T. Horiuchi, N. Kato, K. Sasaki and W. Ueda, *Journal of Solid State Chemistry*, 2010, **183**, 1365-1371.
30. M. Sadakane, T. Horiuchi, N. Kato, C. Takahashi and W. Ueda, *Chemistry of Materials*, 2007, **19**, 5779-5785.
31. L. Zhang, C. Baumanis, L. Robben, T. Kandiell and D. Bahnemann, *Small*, 2011, **7**, 2714-2720.
32. B. T. Holland, C. F. Blanford, T. Do and A. Stein, *Chemistry of Materials*, 1999, **11**, 795-805.
33. S. Meng, D. Li, X. Zheng, J. Wang, J. Chen, J. Fang, Y. Shao and X. Fu, *Journal of Materials Chemistry A*, 2013, **1**, 2744.
34. W. Zhang, J. Zhang, Z. Chen and T. Wang, *Catalysis Communications*, 2009, **10**, 1781-1785.
35. K.-i. Ishibashi, A. Fujishima, T. Watanabe and K. Hashimoto, *Electrochemistry Communications*, 2000, **2**, 207-210.
36. T. Hirakawa and Y. Nosaka, *Langmuir*, 2002, **18**, 3247-3254.
37. H. Bader, V. Sturzenegger and J. Hoigné, *Water Research*, 1988, **22**, 1109-1115.
38. K. Kosaka, H. Yamada, S. Matsui, S. Echigo and K. Shishida, *Environmental Science & Technology*, 1998, **32**, 3821-3824.
39. S. Bayram and L. Halaoui, *Particle & Particle Systems Characterization*, 2013, **30**, 706-714.
40. M. El Harakeh and L. Halaoui, *The Journal of Physical Chemistry C*, 2010, **114**, 2806-2813.
41. M. Wu, J. Jin, J. Liu, Z. Deng, Y. Li, O. Deparis and B.-L. Su, *Journal of Materials Chemistry A*, 2013, **1**, 15491.
42. M. Wu, J. Liu, J. Jin, C. Wang, S. Huang, Z. Deng, Y. Li and B.-L. Su, *Applied Catalysis B: Environmental*, 2014, **150-151**, 411-420.
43. W. Wu, G. Liu, Q. Xie, S. Liang, H. Zheng, R. Yuan, W. Su and L. Wu, *Green Chemistry*, 2012, **14**, 1705.
44. W. Li, D. Li, Y. Lin, P. Wang, W. Chen, X. Fu and Y. Shao, *The Journal of Physical Chemistry C*, 2012, **116**, 3552-3560.
45. W. Zhang, J. Zhang, X. Lan, Z. Chen and T. Wang, *Catalysis Communications*, 2010, **11**, 1104-1108.
46. A. Fujishima, T. N. Rao and D. A. Tryk, *Journal of Photochemistry and Photobiology C: Photochemistry Reviews*, 2000, **1**, 1-21.
47. A. Fujishima, X. Zhang and D. Tryk, *Surface Science Reports*, 2008, **63**, 515-582.

TOC



A facile method to prepare ZnGa₂O₄ photonic crystals with enhanced electronic band absorption and photocatalytic activity.